

Originally published in *Proceedings of the Fifth International Workshop on Compressible Turbulent Mixing*, ed. R. Young, J. Glimm & B. Boston. ISBN 9810229100, World Scientific (1996).

Reproduced with the permission of the publisher.

Criteria for Transition to Turbulence Induced by Richtmyer–Meshkov and Rayleigh–Taylor Instabilities

Zhijian Zhao¹, Nadine Aubry², and Michel Legrand³

¹ Levich Institute for Physico-Chemical Hydrodynamics
The City College of CUNY
New York, NY 10031, USA

² Mechanical Engineering Department
The City College of CUNY
New York, NY 10031, USA

³ Commissariat l’Energie Atomique
Centre d’Etudes de Vaujours-Moronvilliers
BP 7, 77181 Courtry France

Abstract. The aim of this paper is to develop criteria for the transition to turbulence of a mixing zone induced by the Richtmyer-Meshkov and Rayleigh-Taylor instabilities. Our criteria, which make use of quantities defined in the context of biorthogonal decompositions, consist of an exponentially decaying energy spectrum, the saturation of the global entropy function, and quasi-uniform temporal and spatial entropies. We analyze two numerically simulated flows corresponding to a cylindrical explosion generated by explosive. Although these flows are identical, except for slightly different initial conditions, we show by using the previous criteria that their respective evolutions toward a fully-developed turbulent state are rather different.

1 Introduction

Theoretical and experimental studies of the Rayleigh–Taylor (R-T) and Richtmyer–Meshkov (R-M) instabilities show that at large Reynolds number flows, over a wide range of Atwood numbers [1, 2, 3, 4], the R-T instability develops into a turbulent front which, after an initial linear growth described by Taylor [5], seems to be independent of the initial conditions when the front growth starts following a t^2 power law. Whether this self-similar behavior of the front growth can be used as a criterion for turbulence remains an open question. In this paper, we propose alternative criteria, based on the following decompositions.

Biorthogonal decomposition techniques have been proposed as tools for analyzing spatio-temporal complex physical phenomena [6]. They consist in expanding vectorial functions $\vec{V}(\vec{x}, t) = (v_1(\vec{x}, t), v_2(\vec{x}, t), \dots, v_d(\vec{x}, t))$, with $\forall(\vec{x}, t) \in X \times T, \vec{V}(\vec{x}, t) \in R^d, d = 1, 2, 3, \dots$ into orthogonal modes in a Hilbert space $H(X)$ and orthogonal modes in a Hilbert space $H(T)$ for which there is a one-to-one correspondence between the two sets of functions [6]. Such a biorthogonal decomposition of $\vec{V}(\vec{x}, t)$ is the spectral decomposition of the operator U acting from $H(X)$ to $H(T)$ such that

$$\forall \vec{\phi} \in H(X), \quad (U\vec{\phi})(t) = \int_X \vec{V}(\vec{x}, t) \cdot \vec{\phi}(\vec{x}) dm(\vec{x}), \quad (1)$$

where $\vec{\phi}(\vec{x}) \in R^d$. The adjoint operator U^* is defined from $H(T)$ to $H(X)$ as

$$\forall \psi \in H(T), \quad (U^*\psi)_i(\vec{x}) = \int_T v_i(\vec{x}, t) \psi(t) d\tilde{m}(t) \quad (2)$$

for $i = 1, 2, \dots, d$. In this definition, $dm(\vec{x})$ and $d\tilde{m}(t)$ denote the measures defining the scalar product in $H(X)$ and $H(T)$, respectively.

If U has a point spectrum, the decomposition takes the form

$$\vec{V}(\vec{x}, t) = \sum_{i=1}^N A_n \psi_n(t) \vec{\phi}_n(\vec{x}) \quad (3)$$

where $A_1 \geq A_2 \geq \dots \geq A_N > 0$,

and $(\vec{\phi}_n, \vec{\phi}_m)_{H(X)} = (\psi_n, \psi_m)_{H(T)} = \delta_{nm}$.

The eigenmodes $\vec{\phi}_n(\vec{x})$ and $\psi_n(t)$ are related by the operator U : $U\vec{\phi}_n = A_n\psi_n$ (and $U^*\psi_n = A_n\vec{\phi}_n$). The relation between the spectral decomposition of U and that of the correlation operator U^*U (or UU^*) is straightforward [6, 7]. The former can thus be understood as a deterministic version of the proper orthogonal decomposition [8].

In the sense of the two norms previously introduced, two global averaged quantities, the energy and the entropy, can be defined. The energy is simply the sum of the squares of the eigenvalues

$$E = \sum_{n=1}^N A_n^2, \quad (4)$$

while the entropy [6] is defined as

$$H = -\frac{1}{\log N} \sum_{n=1}^N p_n \log p_n, \quad (5)$$

where p_n is the normalized eigenvalue $p_n = A_n^2/E$. The entropy quantitatively measures the degree of space-time complexity of $\vec{V}(\vec{x}, t)$. If the energy is uniformly distributed

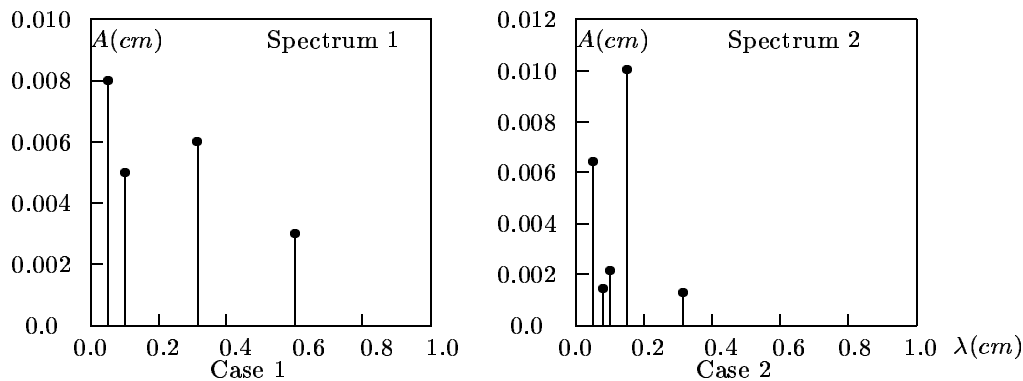


Figure 1: Fourier spectrum of the initial interfacial perturbation.

among all modes, then the entropy is maximal, equal to one. Likewise, if only a single mode is excited, the entropy is zero.

Two other quantities, the spatial and temporal entropies, have also been introduced [6]. The spatial entropy measures the spatial degree of complexity at each instant. It is defined as

$$H_S(t) = -\frac{1}{\log N} \sum_{n=1}^N p_{\psi_n}(t) \log p_{\psi_n}(t) \quad (6)$$

where the temporal functions p_{ψ_n} are

$$p_{\psi_n}(t) = \frac{A_n^2 |\psi_n(t)|^2}{E_S(t)}, \quad (7)$$

$E_S(t)$ being the spatial energy of the flow evolving in time,

$$E_S(t) = \sum_{n=1}^N A_n^2 |\psi_n(t)|^2.$$

Similarly, a temporal entropy measuring the degree of complexity in the time series, at each spatial position, is

$$H_T(\vec{x}) = -\frac{1}{\log N} \sum_{n=1}^N p_{\phi_n}(\vec{x}) \log p_{\phi_n}(\vec{x}) \quad (8)$$

where the spatial functions p_{ϕ_n} are

$$p_{\phi_n}(\vec{x}) = \frac{A_n^2 |\vec{\phi}_n(\vec{x})|^2}{E_T(\vec{x})}, \quad (9)$$

$E_T(\vec{x})$ being the temporal energy of the flow, spatially evolving,

$$E_T(\vec{x}) = \sum_{n=1}^N A_n^2 |\vec{\phi}_n(\vec{x})|^2.$$

2 Detection of a Self-Similar State

In the previous framework, a space-time symmetry naturally appears as a pair of operators (\tilde{S}, S) , \tilde{S} acting on $H(T)$ and S acting on $H(X)$, which intertwines the operator U defined in (1), i.e. $\tilde{S}U=US$ (and, similarly, $SU^* = U^*\tilde{S}$). The argument can be generalized to a space-time self-similarity satisfying

$$US = \gamma\tilde{S}U, \quad (10)$$

$$SU^* = \gamma^{-1}U^*\tilde{S} \quad (11)$$

where γ is different from one.

A necessary and sufficient condition for a flow to be self-similar (10), (11) is the exponential decay of a subset of eigenvalues, i.e.

$$A_{k+1} = \gamma A_k, \quad k \in \mathbb{N}. \quad (12)$$

Then, the corresponding spatial and temporal eigenmodes are related via the pair of operators (S, \tilde{S}) such that

$$\vec{\phi}_{k+1} = S\vec{\phi}_k, \quad \psi_{k+1} = \tilde{S}\psi_k. \quad (13)$$

Assuming that the flow, in its turbulent state, satisfies the scaling symmetries of the Navier-stokes equations [10], the flow is self-similar in the sense of (10), (11) and the operator S and \tilde{S} are dilation symmetries

$$(S\vec{\phi})(x) = \vec{\phi}(\lambda^{-1}x) \quad (14)$$

$$(S\psi)(t) = \psi(\lambda^{-1}\gamma t). \quad (15)$$

Once self-similarity takes place, the global entropy should become independent of the time domain considered in the definition of the operator U (1), namely H considered over subdomains $(0, \tilde{T})$ should saturate for large values of \tilde{T} . Furthermore, as small

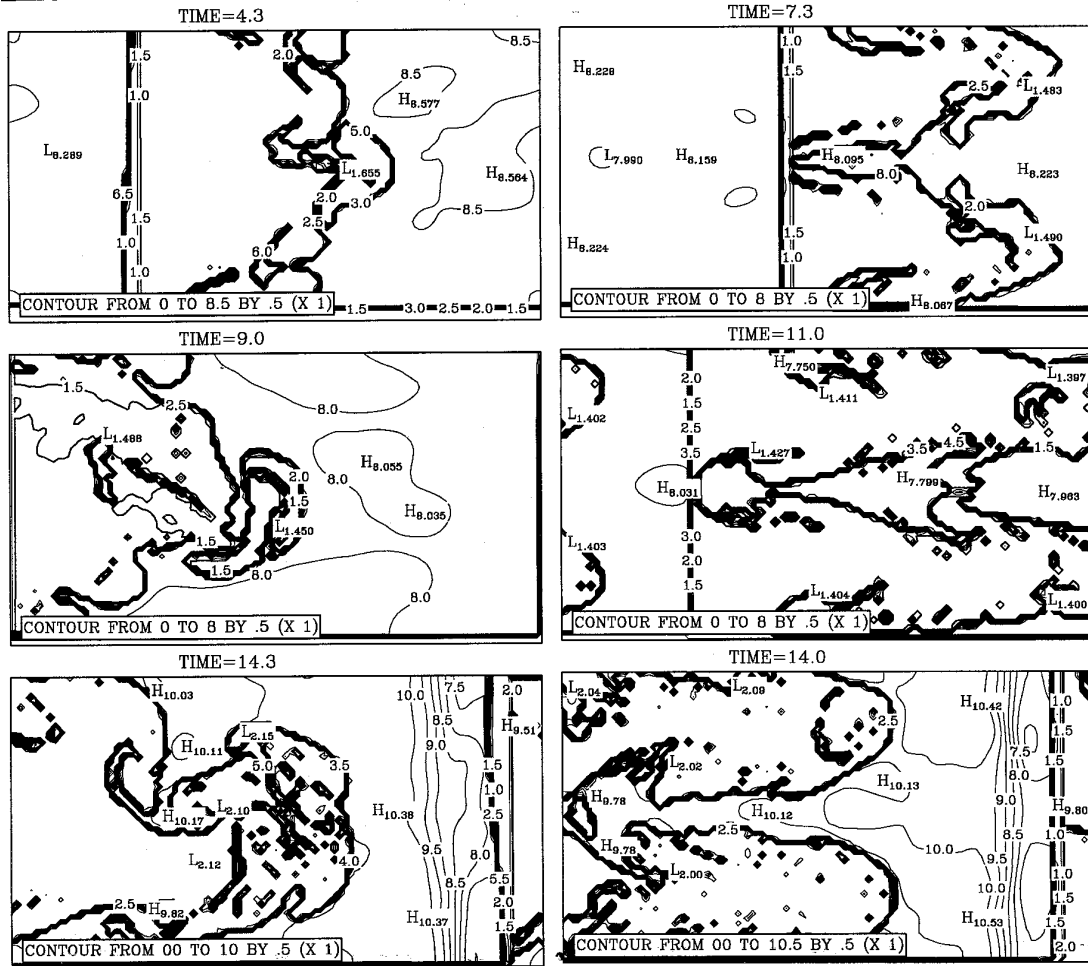


Figure 2: The density field in both cases (time unit : microsecond); Case 1 (left) and Case 2 (right).

scales gain energy, the slope of the eigenspectrum decreases, the entropy increases and the temporal and spatial entropies become more uniformly distributed in space and time.

One can then distinguish two types of criteria. The first type, Criteria 1, permits the comparison between two different flows.

Criteria 1 As a control parameter varies and the flow becomes more and more turbulent,

- the eigenspectrum becomes flatter;
- the saturated global entropy increases;
- the temporal/spatial energies and entropies become more uniformly distributed in space and time.

The second type, Criteria 2, permits the detection of a transition time within a given flow.

Criteria 2 Two necessary conditions for the flow to be considered turbulent at a certain time T_t are:

- at T_t and beyond, the global entropy has reached a quasi-saturation level;
- at T_t and beyond, the spatial entropy does not exhibit large scale variations.

3 Application to Simulated RT and RM Flows

In this section, we analyze two simulated R-T and R-M flows, referred to as case 1 and case 2, respectively. These flows correspond to the same basic physics: a cylindrical implosion generated by explosive observed via axial radiography. Implosion is initiated by a cylindrical detonation wave converging in the explosive cylinder. The two cases differ only by the Fourier content of the initial interfacial perturbation between the two fluids (see Fig. 1). The binary interface with small initial defects, impulsively driven by a shock wave, is subject to a R-M instability, followed by a long R-T phase, which leads to the formation of a mixing zone between the two fluids. The computations are performed in a 2-D rectangular domain with the Eulerian code 2D EAD which solves the Euler equations [12]. Fig. 2 shows the density field in both cases.

We now perform the biorthogonal analysis (1) of the velocity and density of the flows, particularly seeking the presence of a self-similar (inertial) range of the spectra. Fig. 3(a) shows that the velocity spectrum decays more slowly in Case 2 than in Case 1. Both spectra, plotted in a logarithmic scale, exhibit an approximately exponential decay in their “inertial range”, characteristic of self-similarity and fully developed turbulence. Moreover, a more detailed plot (not shown here) reveals that the spectrum in Case 1 exhibits an order 2 degeneracy, reminiscent of a traveling wave (or a modulated traveling wave [13]). Such a degeneracy has disappeared in Case 2.

We now compare the global entropy and the mixing length variations in both cases (see Figs. 3(b),(c)). The entropy reveals that there are three stages in the evolution

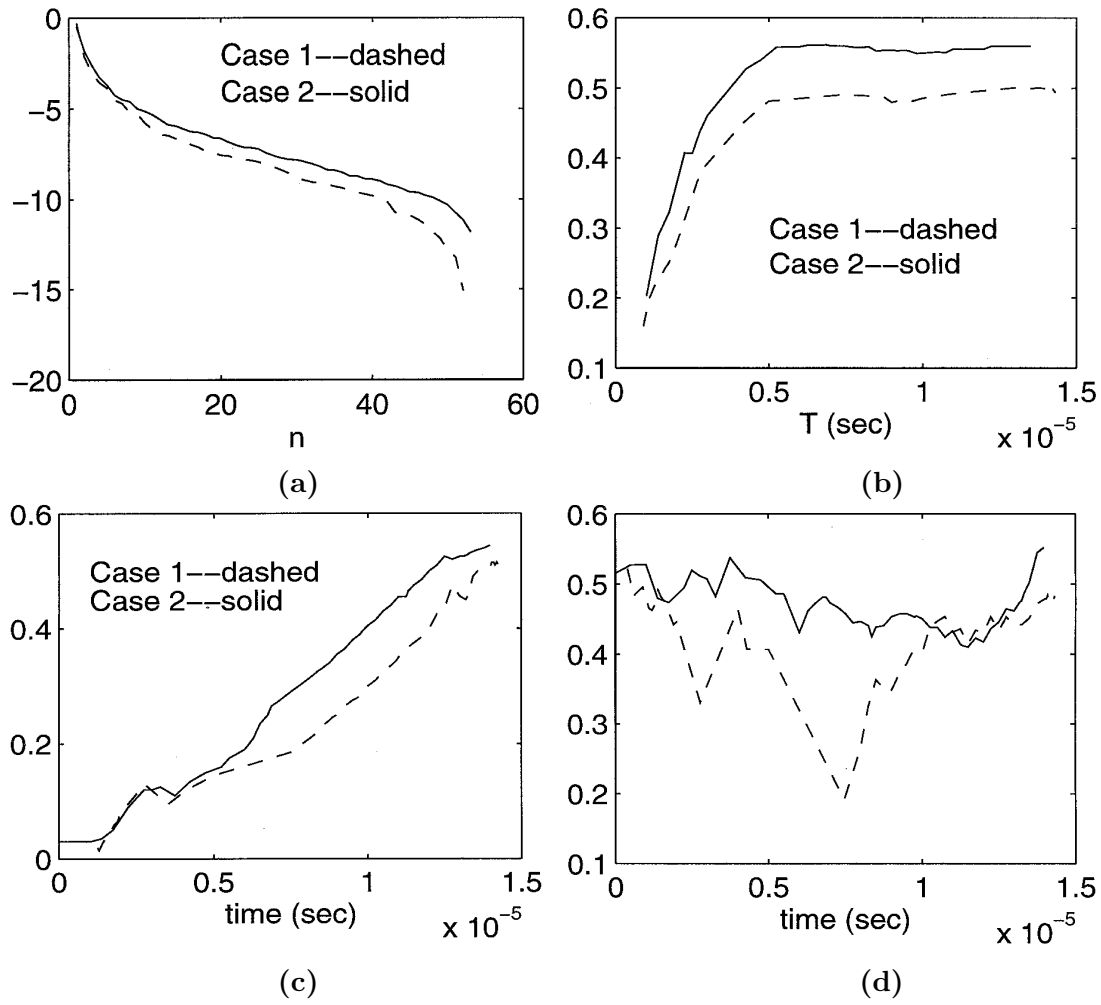


Figure 3: (a) Eigenspectrum of the velocity. (b) Global entropy of the density. (c) Square root of the MZW. (d) Spatial entropy of the density.

of the flows toward turbulence: (a) until time $t = 3\mu\text{sec}$, both the mixing zone width (MZW), δ , and the global entropy, H , grow linearly; (b) this linear growth is followed by a nonlinear variation of $\sqrt{\delta}$ with time, as well as a quasi-quadratic growth of the global entropy; (c) in the final stage, the growth of $\sqrt{\delta}$ becomes a linear function of time, while H increases slowly and reaches saturation. A comparison between the two flows shows that both the saturated entropy and the final mixing length are larger in Case 2 than in Case 1, suggesting that the former flow is more turbulent.

The spatial and temporal entropies of the density in the two cases are compared in Figs. 3(d), 4, and 5. Fig. 3(d) shows that the spatial entropy is larger and flatter in Case 2 than in Case 1, indicating a high small scale intensity in the turbulent mixing processes of the flow. Fig. 4 displays the spatial distribution of the temporal entropies. It is clear that the temporal entropy is more uniform in Case 2 than in case 1. Fig. 5 displays the temporal entropy of the streamwise velocity in both cases: characteristic scales are smaller in Case 2 than in Case 1.

4 Concluding Remarks

We have compared two simulated implosive flows involving R-T and R-M instabilities. The flows differ only by the shape of the initial interfacial perturbation. As time increases, the flows experience an initial linear growth followed by a non-linear dynamical stage which becomes turbulent as the t^2 growth of the mixing zone width develops. After that time, the global entropies of the flows saturate.

All the results of our analysis converge to identify Case 2 as the most turbulent flow. Indeed, Case 2 exhibits

- the largest mixing zone width, growing with time proportionally to t^2
- the largest saturated global entropy
- the highest intensity of small scale fluctuations, together with quasi-uniform distributions of temporal/spatial energies and entropies
- the flattest spectrum, decaying approximately exponentially in its "inertial range".

In Case 2, the flow can be considered turbulent at $T_t=7.5 \mu\text{sec}$ and beyond. Indeed, after T_t ,

- the mixing zone width grows with time as t^2
- the global entropy has reached its quasi-saturation level
- the spatial entropy does not exhibit large scale variations.

References

- [1] K. I. Read and D. L. Young, "Experimental Investigation of Turbulent Mixing by Rayleigh-Taylor Instability", AWE Report, 011/83 (1983).

- [2] J. M. Redondo and P. F. Linden, "Mixing Produced by Rayleigh-Taylor Instabilities", Proceedings of Waves and Turbulence in Stably Stratified Flows, IMA Conference, Leeds (1989) (Ed. J. King and S. D. Mobbs).
- [3] S. B. Dalziel, "Perturbations and Coherent Flow in Rayleigh-Taylor Instability", 4th International Workshop on the Physics of Compressible Turbulent Mixing, (1993) (Ed. by P. F. Linden, D. L. Youngs & S. B. Dalziel).
- [4] J. Glimm, X. L. Li, and Q. Zhang, International Workshop on the Physics of Compressible Turbulent Mixing, Conf-8810234, National Tech. Serv., U.U. Dept Com, 5285 Port Royal, Springfield, VA 22161, 607-626, (1992).
- [5] G. I. Taylor, Instability of Superimposed Fluids, Proc. Royal Soc. (1950).
- [6] N. Aubry, R. Guyonnet, and R. Lima, J. Stat. Physics 64:683-739, (1991).
- [7] N. Aubry, Theoretical and Computational Fluid Dynamics 2: 339-352 (1991).
- [8] J. L. Lumley, Stochastic Tools in Turbulence, Academic (1970).
- [9] N. Aubry, R. Guyonnet, and R. Lima, J. Nonlinear Sci. 2: 183-215 (1992).
- [10] N. Aubry, R. Guyonnet and R. Lima, J. Stat. Phys. 67:203-228 (1992).
- [11] M. Legrand and N. Toque, 3rd International Workshop on the Physics of Compressible Turbulent Mixing, 9-18, (1991).
- [12] M. Legrand and N. Toque, 4th International Workshop on the Physics of Compressible Turbulent Mixing, 568-577, (1993).
- [13] N. Aubry and R. Lima, Chaos 5: 578-588, (1995).

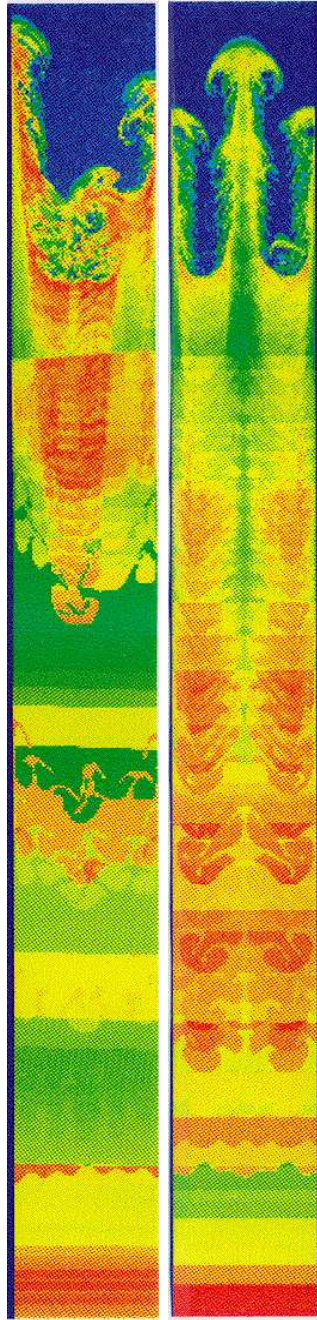


Figure 4: Temporal entropy of the density. Case 1 (left) and Case 2 (right).

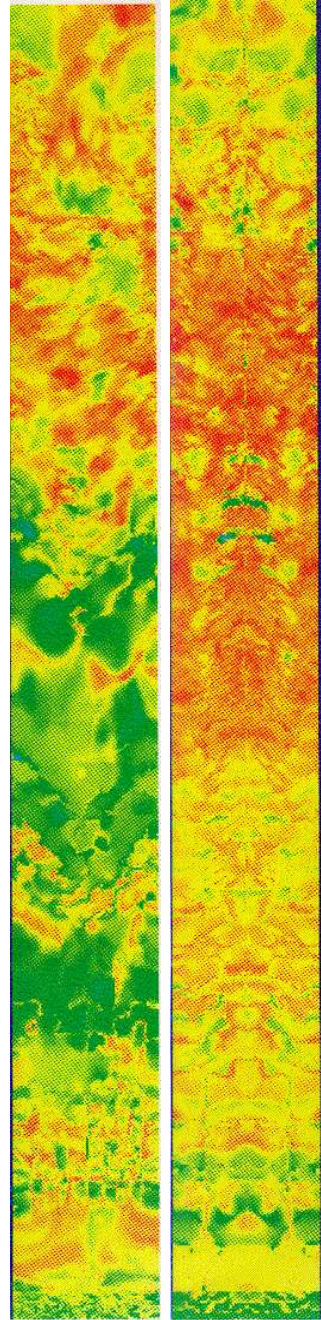


Figure 5: Temporal entropy of the velocity. Case 1 (left) and Case 2 (right).